IV Journeys in Multiphase Flows (JEM2015)
March 23-27, 2015 - Campinas, Brazil

PaperID: JEM-2015-XXXX

A COMPUTATIONAL STUDY OF THE INTERFACIAL HEAT TRANSFER IN SPHERICAL AND DEFORMED FLUID PARTICLES

Rafael Franklin Lazaro de Cerqueira
Emilio E. Paladino
Clovis R. Maliska
SINMEC - Computational Fluid Dynamics Lab
Mechanical Engineering Department
Federal University of Santa Catarina
88040-900 – Florianopolis – SC – Brazil
rafaelfc@sinmec.ufsc.br, paladino@sinmec.ufsc.br

Abstract. *In this paper, the interfacial heat transfer process of spherical and distorted fluid particles is studied through the Volume-Of-Fluid approach, aiming the development of closure correlations for the two-fluid model in heat and mass transfer problems. The Nusselt numbers of spherical particles are compared with the usual correlations presented in literature to validate the numerical model. From the methodology adopted in this work is possible to perform an analysis of the flow and thermal field around the fluid particles and study the effect of different morphologies on the global heat transfer coefficients. It is shown that the interfacial heat flux distribution is affected by the particles shape, inducing changes in the flow and thermal fields around the fluid particle and consequently leading differences in total heat transfer rate.*

Keywords: *Interfacial Heat Transfer, Distorted bubbles, CFD*

1. INTRODUCTION

Gas-liquid two-phase flows are frequently encountered in the oil, chemical and energy transformation industries. Some specific applications in oil and gas industry related to flow assurance problems, such as wax deposition, hydrate formation and corrosion problems by CO_2 and HS_2 among others, require, in addition to the interfacial momentum transfer, the detailed modeling of the heat and mass transfer processes between phases. In the chemical industry, the need of these detailed modeling is necessary in the design of bubble column reactors, as shown in (Kantarci *et al.*, 2005). These flows usually includes multicomponent systems where mass transfer processes are linked to concentration gradients.

Bubbles of different sizes and shapes are encountered in several flow patterns, ranging from spherical ones in finely dispersed bubbly flow to Taylor bubbles in slug flow. Even in slug flow pattern, small dispersed bubbles flow within the liquid slug between two consecutive Taylor bubbles. The simulation of these flows requires precise closure models for interfacial transfer, even in an one-dimensional approaches, utilized in flow wells or multi-dimensional models, employed in the modeling of the flow inside pumps, separators and other elevation components and primary oil treatment. For the case of momentum transfer, several closure relations have been presented in literature (Ishii and Hibiki, 2011; Clift *et al.*, 1978) including correlations for the the cases of distorted bubbles. On the other hand, in modeling interfacial heat and mass transfer processes, in the application of the two fluid models for dispersed flow patterns the usual practice is to employ consolidated correlations based on Re and Pr or Sc dimensionless groups, but considering perfectly spherical shaped bubbles, which is not always true in several real applications.

Ranz and Marshall (1952) conducted an experimental investigation of the rate of evaporation of spherical liquid drops, verifying the analogy between heat and mass transfer, and proposing a simple correlation accounting for diffusion and forced convection of mass and heat transfer. For bubbles, (Lochiel and Calderbank, 1964) proposed correlations using the boundary layer theory, including the effect of internal circulation, for fluid spheres, spheroids and spherical cap shapes with mobile and immobile interfaces when $Pe(Pe = Re \cdot Sc$ or $Re \cdot Pr)$ and Sc are larges. A similar correlation was proposed by (LeClair and Hamielec, 1971) for spherical fluid particles for different ranges of Pe and Sc. In the work of Oellrich *et al.* (1973), the authors propose a correlation for spherical bubbles from the results obtained of the mass transfer numerical investigation from a previously obtained velocity field. Takemura and Yabe (1998) proposed a correlation based in the modification of an equation given by (Clift *et al.*, 1978), employing their numerical and experimental results from the dissolution of gas bubbles in different silicon oils. Furthermore, the heat and mass transfer between phases in bubbly flow regime is still not fully understood and is a topic of ongoing research (Hayashi *et al.*, 2014; Bothe and Fleckenstein, 2013; Aboulhasanzadeh *et al.*, 2013, 2012; Marschall *et al.*, 2012).

The main difficult in modeling multiphase, multicomponent and non-isothermal flows is the interface tracking and its definition, as well the transfer mechanism and calculation between the two (or more) distinguished domains. Most of the recent numerical works exploring the interfacial heat and mass transfer utilizes interface or front tracking methodolo-

gies, such as Volume-Of-Fluid (Bothe and Fleckenstein, 2013), Level-Set (Wang *et al.*, 2008) and other Front-Tracking methods (Aboulhasanzadeh *et al.*, 2012). For the interfacial transfer mechanism, several approaches have been proposed in literature. In the recent paper of Marschall *et al.* (2012), the authors propose a new method for the calculation of the interfacial mass transfer fluxes, called the Continuous-Species-Transfer (CST) which is based on an analogy of the the well-known Continuous-Surface-Force (CSF) Method from Brackbill *et al.* (1992). Another alternative to calculate the mass and heat transfer is to utilize the overall energy or mass balance concept, as showed in (Hase and Weigand, 2004) and (Wang *et al.*, 2008). Recently, some authors proposed multiscale methods, which, in general, are based on the use of know solutions, based on boundary layer theory, to predict the interfacial transfer in the near interface regions, to save computational effort in DNS computations (Aboulhasanzadeh *et al.*, 2012, 2013) and to capture the steep concentrations gradients that appears in the interface (Bothe and Fleckenstein, 2013). Aboulhasanzadeh *et al.* (2013) showed that the mutiscale approach presents good agreement when compared to experimental results, in spite of its various assumptions.

Another alternative in modeling interfacial heat transfer is to employ body fitted grids with increased resolution near the fluid particle surface. Figueroa-Espinoza and Legendre (2010) studied the mass transfer of a spheroidal bubble rising through a stationary liquid for various flow and geometrical configurations, analyzing the local and global mass transfer. A huge disadvantage of such approach is the fact that the interface morphology is imposed, while in the reality is a result of the balance between the inertial, viscous and superficial forces, not allowing the obtained results to be linked with the adequate dimensionless parameters that describes the phenomena. An important remark in the work of Figueroa-Espinoza and Legendre (2010) is the discussion about the applicability of mass transfer correlations in the Two-Fluid Model (TFM) by correction factors due to the deviations from a spherical shape.

The main objective of the present work is to determine, through a detailed modeling of the flow around bubbles with different interface shapes, the interfacial heat and mass transfer coefficients in non-isothermal multiphase flows and how the interface shape affects the process and, ultimately, the global heat and mass transfer coefficients, which are needed for the Two-Fluid Model closure.

2. METHODOLOGY

To accomplish the objective previously defined, the detailed flow structure around individual bubbles was studied through the Volume-of-Fluid (VOF) method (Hirt and Nichols, 1981). In the VOF method, the phases are defined with the aid of an indicator function α_b advected in a fixed mesh, whose value varies from $\alpha_b = 0$ to $\alpha_b = 1$. If $\alpha_b = 1$ the value indicates the presence of the fluid particle phase, the continuous phase presence is given by $\alpha_b = 0$ and intermediate values are treated as interface cells. The interface was geometrically reconstructed by the Piecewise Linear Interface Construction (PLIC) scheme (Youngs, 1982), improving the fluxes between the mesh cells.

For the momentum equation, the chosen surface stress model was the Continuous Surface Stress (CSS) (Lafaurie *et al.*, 1994). The phases are modeled as incompressible and viscous in a laminar flow. The simulations presented in this work were developed in ANSYS FLUENT CFD 15.0.

From the generalized graphical correlation shown in (Clift *et al.* (1978), p. 27) the bubble shape can be predicted by the use of some characteristic dimensionless numbers, these are the Eötvös (Eo), Reynolds (Re) and Morton (Mo).

$$Eo = \frac{g\left(\rho_c - \rho_b\right) d_b}{\sigma / d_b}, \tag{1}$$

$$Re = \frac{\rho_c U_{tb} d_b}{\mu_c}, \tag{2}$$

$$Mo = \frac{g \mu_c^4 \left(\rho_c - \rho_b\right)}{\rho_c^2 \sigma^3}, \tag{3}$$

where ρ is the density, μ is the viscosity, σ is the surface tension, U_{tb} is the bubble terminal velocity, d_b is the bubble diameter, whose calculation will be shown later. The subscripts b and c represent, the bubble and the continuous phase, respectively.

Another important dimensionless number in the heat transfer analysis is the Prandtl number (Pr) that gives the relation of momentum and thermal diffusivity,

$$Pr = \frac{C_{p_c} \mu_c}{k_c}, \tag{4}$$

where C_{p_c} is the continuous specific heat capacity and k_c is the continuous thermal conductivity.

Along with fore mentioned dimensionless numbers, four other characteristic dimensionless numbers are the density ratio ($\gamma = \rho_b / \rho_c$), the viscosity ratio ($\kappa = \mu_b / \mu_c$), the thermal conductivity ratio ($\beta = k_b / k_c$) and the specific heat capacity ratio ($\lambda = C_{p_b} / C_{p_c}$)

In the analysis of the heat transfer between the phases, the results presented in this work will be expressed by the Nusselt number (Nu),

$$Nu = \frac{hd_b}{k_c}, \tag{5}$$

where h is the heat transfer coefficient.

In a heat transfer analysis, the common practice to obtain the heat transfer coefficient h value is to employ a heat balance at the interface in the following manner,

$$h = \frac{-k_c}{S\Delta T}\left.\frac{\partial T}{\partial \hat{n}}\right|_{\text{interface}} \tag{6}$$

where $\hat{n}$ is normal vector pointing outward the interface, ΔT is a temperature difference and S is the interfacial surface area.

However, one of the shortcomings of the interface tracking through implicit methods, such as VOF, Level-Set or CLSVOF (Coupled Level-Set Volume-of-Fluid), is that the interface position is not exactly defined. Although the mesh refinement lead to a more accurate capture of the interface position, a problem arises in the explicit calculation of the interfacial heat fluxes. Since the VOF model treats the two or more phases in a continuous point of view, the high gradients of both temperatures and fluid transport properties encountered at the interface, are dependent of the volume fraction (or the level-set function) when evaluated for the mixture. This dependence can be seen in Fig. 1 where the dimensionless local Nusselt (Eq. (14)), tangential velocity (Eq. (15)) along the interfaces (calculated with $\alpha_b = 0.1$, $\alpha_b = 0.3$ and $\alpha_b = 0.5$) are given. As seen, the interface position and the velocity profiles show almost none discrepancies, while the local Nusselt for the three ϕ values do not coincide at the particles front hemisphere, where the heat fluxes are stronger. Although the values are not the same, they show the same tendency and are of fundamental importance to support the physical analysis and conclusions about the global results obtained.

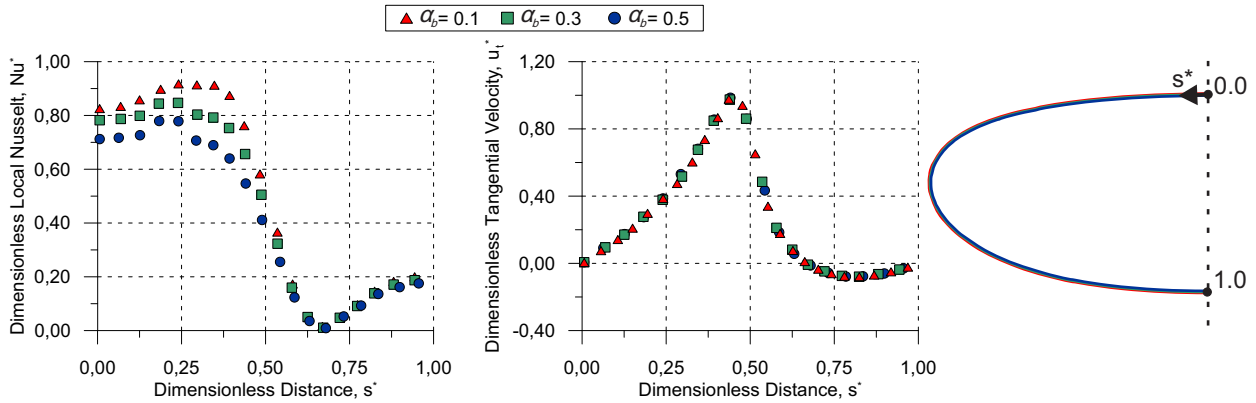

Figure 1. Dimensionless local Nusselt number Nu^* and dimensionless tangential velocity $u_t{}^*$ for the interfaces obtained for different α_b values.

The calculation of the interfacial heat fluxes are also difficult in explicit interface tracking methods, such as Lagrangian approaches based on immersed boundary methods (Aboulhasanzadeh *et al.*, 2012), where the transport equations are resolved in a fixed the background mesh and, again, the fluxes at the interface cannot be explicitly calculated, even when the position of the interface is explicitly determined. None of these methods cannot handle sharp variations of the transport properties. The only approaches which allows the explicit calculation of interfacial fluxes are those based on the interface fitted grid.

In addition, when calculating the heat transfer coefficient h (Eq. (6)) a reference temperature is required at the interface, T_s. Once the temperature variation across the interfacial region is sharp in the VOF method, the interfacial temperature T_s cannot be easily defined.

In order to avoid the problems described in the above paragraphs, the Nusselt Nu number was obtained from a global balance, which maintained the particle temperature constant by the inclusion of a source term S_h in the energy conservation equation, via FLUENTs User Defined Functions(UDF). This source term was equal to the total heat transferred in the previous timestep Δt, from the bubble to the continuous phase. Equation (7) is the source term added to the energy conservation equation

$$S_h = \alpha_b \rho_b C_{Pb} \frac{\left(T_b - T^{t-\Delta t}\right)}{\Delta t} \tag{7}$$

where T_b is the bubble temperature defined in the beginning of each simulation run and $T^{t-\Delta t}$ is the temperature in the previous timestep. The term α_b in Eq. (7) ensures that the source term only exists in the fluid particle domain, seeing that α_b has zero value outside the fluid particle and $0 < \alpha_b \leq 1$ inside.

With the aid of this source term, T_b remained constant during the whole simulation time due to the fact that a small time step Δt was chosen. As a result, the reference temperature difference($\Delta T = T_b - T_c$) was simply made equal to the temperature of the bubble T_b minus the temperature of the liquid far from the interface T_c (which is equal to the initial liquid temperature).

Employing an energy balance in a control volume $V.C.$ large enough to enclose the bubble interface, it was possible to calculate the total heat $\dot{Q}$ transferred from the dispersed to the continuous phase through the integration of S_h resulting in $\dot{Q} = \int_{V.C} S_h dV$. In this fashion, the global Nusselt number, is defined by

$$Nu_{global} = \frac{\dot{Q} d_b}{S\,(T_b - T_c)\,k_c} \tag{8}$$

The analysis of the local Nusselt number along the interface Nu_{local} is important in order to understand some phenomena related to local flow pattern as, for instance, the separation point of the boundary layer, behind the fluid particle. The Nu_{global} was calculated through the explicit calculation of the interfacial fluxes assuming an interface position, which is defined as the iso-surface where $\alpha_b = 0.1$, and the convective heat transfer coefficient h was calculated with Eq. (6), then,

$$Nu_{local} = \frac{h d_b}{k_c}. \tag{9}$$

The resulting local Nusselt number was non-dimensionalized by the difference between the maximum and minimum values of the Nu_{local} number (Eq. (14)) in the analysis presented in this work.

Although the resulting Nu_{local} numbers calculated in this way can be only considered as qualitative parameters, the same methodology was used in all cases, allowing a qualitative comparison of the local phenomena among the different cases.

To simulate the process of a rising bubble in a infinite media, the computational domain and the boundary conditions were defined according to the scheme shown in Fig. 2.

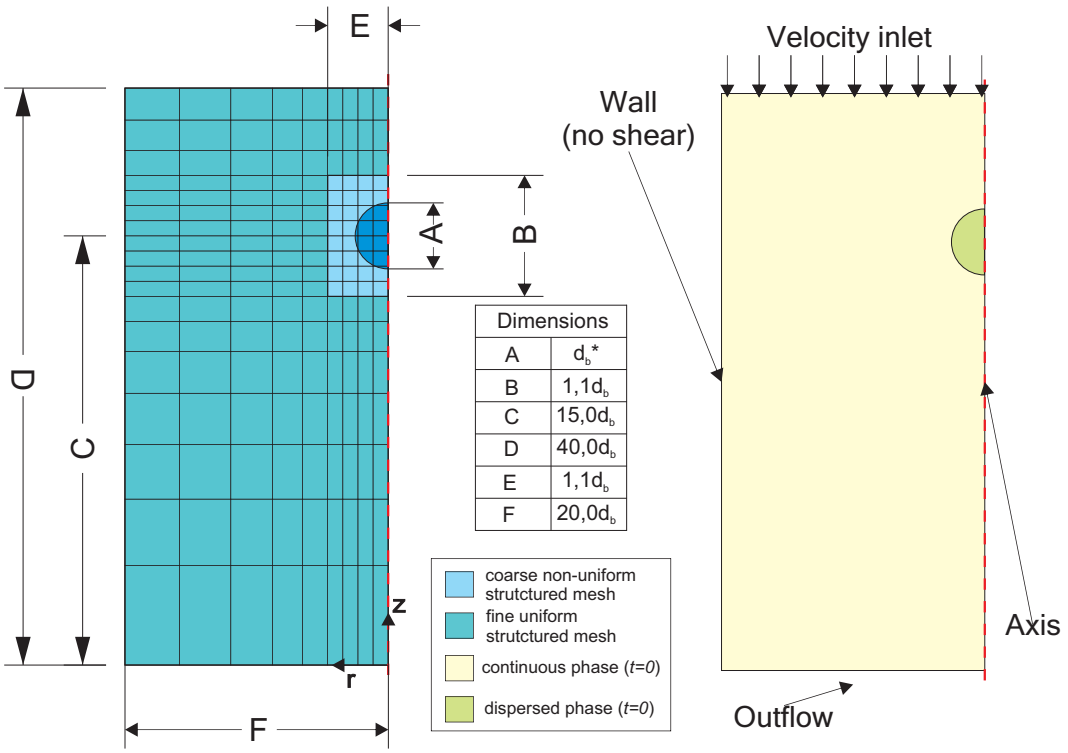

Figure 2. Computational domain scheme, boundary and initial conditions.

In this work, the governing equations are solved with the reference coordinate system fixed on the fluid particle. Employing this reference coordinate system, it was possible to reduce the computational domain, once it was only needed to enclose a relative small domain around the fluid particle, when comparing the computational domain required for a inertial coordinate system. This allowed for a better mesh refinement, specially near the fluid particle, where the transfer

of heat and momentum occurs, enhancing the quality of the results and allowing the bubble to rise for large periods of time with no physical limitation.

In order to include the effects of the fluid particle acceleration, a source term was added to the momentum conservation equation via FLUENTs User Defined Functions(UDF). First, an average bubble rise velocity ${U_b}^t$ was calculated, in a instant of time t as

$$ {U_b}^t = \frac{\int \alpha_b u \, d\Omega}{\int \alpha_b \, d\Omega} \tag{10} $$

where Ω is the computational domain and u is the axial component of velocity $\vec{u}$. It is important to mention, that the volumes with $0 < \alpha_b \leq 1$ where approximately the ones enclosing the dispersed phase (fluid particle) and the calculations were performed after each time step was converged. This ${U_b}^t$ was then introduced to the U_{inlet} as $U_{inlet} = -{U_b}^t$ in the top boundary condition (see Fig.2) at the new instant of time $t + \Delta t$. A new average bubble rise velocity ${U_b}^{t+\Delta t}$ was obtained at this time instant. The bubble acceleration in each time step was evaluated as,

$$ a_{bubble} = \frac{{U_b}^{t+\Delta t} - {U_b}^t}{\Delta t} \tag{11} $$

In this way, the source term introduced in the momentum conservation equation $S_m = -\rho \, a_{bubble}$ and was applied to each volume of the computational domain to remain the bubble stationary.

For the cases of deformed fluid particles, it was necessary to define an equivalent bubble diameter to obtain some of the dimensionless parameters presented in the equations above. This bubble diameter d_b was defined as the equivalent diameter from a spherical bubble, such that

$$ d_b = \sqrt[3]{\frac{6V_s}{\pi}} \tag{12} $$

derived from the volume from a sphere ($\pi d^3/6$) and a calculated bubble volume V_s.

Some studies were made to ensure that the the simulations were performed free of wall effects and to check if the outflow and inlet boundaries were well positioned, in order to obtain a far field approximation. In this manner, the resulting computational domain is sketched in the Fig. 2 with its dimensions evaluated as a function of the bubble diameter d_b. To simulate the rising bubble, the bubble initial shape was defined as a sphere with diameter d_b placed $15d_b$ away from the bottom. In the interest to reduce the computational effort, the mesh was subdivided in two different regions, a smaller fine region with an uniform structured mesh followed by a larger coarse non-uniform structured mesh. The transition between the regions was made smooth with the help of a spline function.

3. RESULTS AND DISCUSSIONS

3.1 Numerical Simulations

In order to study the effect of the bubble shape on the heat transfer process, it was necessary to develop studies for situations located in the three distinct regions of the bubble shape regimes: i) spherical; ii) ellipsoidal and iii) ellipsoidal-cap, as presented (Clift *et al.* (1978), p. 27). These points are plotted in Fig. 3.

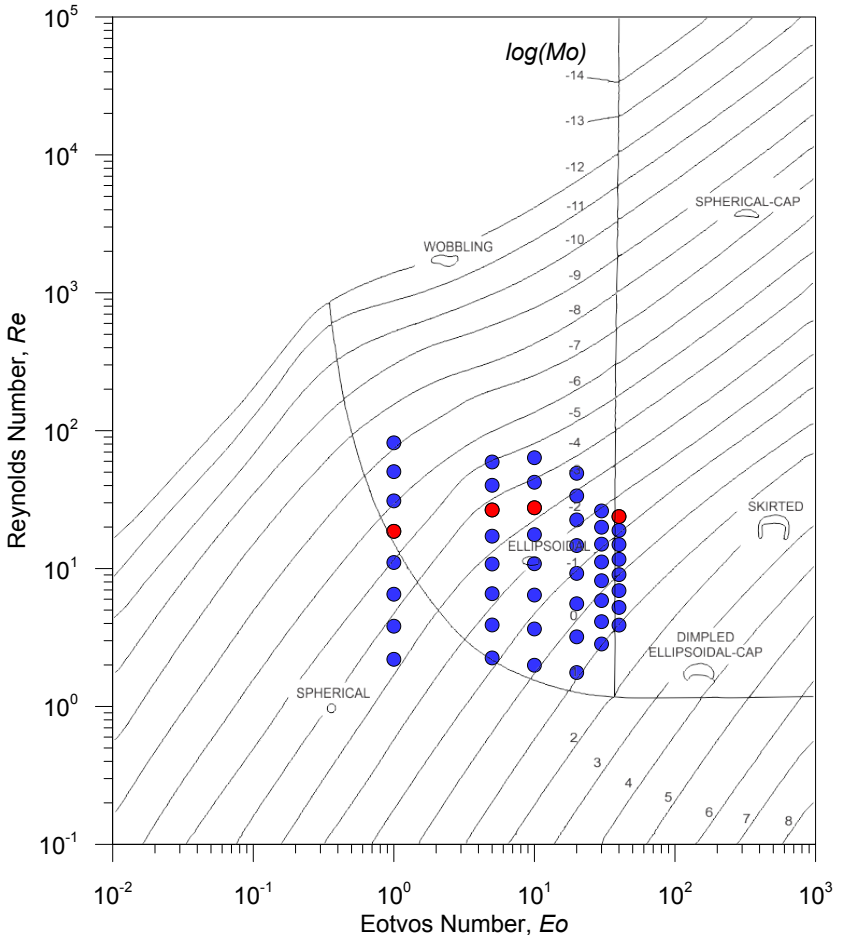

Figure 3. Simulations performed in this work plotted in the map presented in (Clift *et al.* (1978), p. 27) for different Pr values.

From Fig. 3, it is possible to predict the Reynolds Number Re based on the terminal bubble rise velocity U_{tb} and the bubble shape from a pair of Eötvös Eo and Morton Mo numbers.

Here, the obtained bubble morphologies agreed well with the encountered bubble map, additionally the Re obtained in the steady state regime suffered little deviations from the expected values.

The simulations were performed for a pair of Eötvös Eo and Morton Mo numbers with for different Pr values: i) $Pr = 0.25$; ii) $Pr = 0.50$; iii) $Pr = 0.75$; iv) $Pr = 1.00$; v) $Pr = 2.50$; vi) $Pr = 5.0$ and vii) $Pr = 10.0$.

3.2 Mesh convergence test

A mesh refinement study was made to ensure that simulations were performed free of discretization error and the computational mesh was capable to capture the boundary layer effects, once the interfacial heat and momentum transfer occurs in this region.

Based on the fact that higher the Re, thinner is the momentum boundary layer and the Pr number gives the relation of the momentum and thermal boundary layer in a inverse proportion, i.e. higher the Pr, smaller is the thermal boundary layer, the mesh convergence study was made for the higher Mo in each Eo – the higher Re in each Eo – with $Pr = 10.0$.

The number of volumes accounted in the mesh refinement study are those of the fine region (see Fig. 2), $N_{vol} = (1.1d_b)(1.1d_b)/\Delta l^2$, where $\Delta l = \Delta x = \Delta y$ is the finite volume size in the fine region. Below in Fig. 4 is the Nu_{global} values for the different mesh sizes.

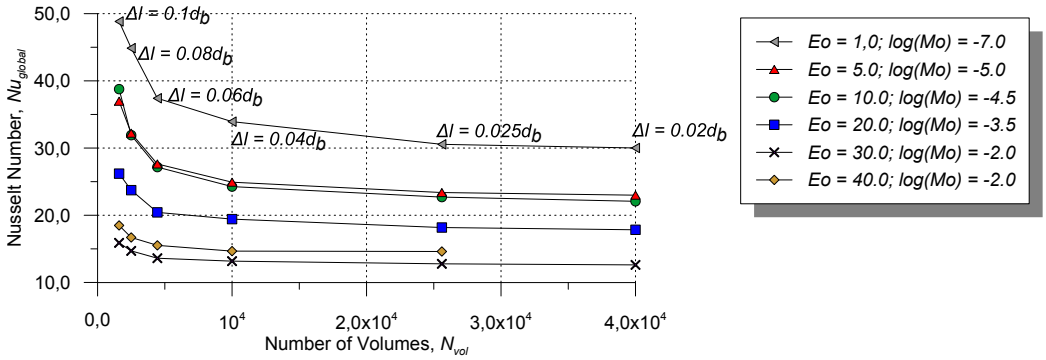

Figure 4. Mesh convergence study for the higher Re in each Eo with $Pr = 10.0$.

Figure 4 shows that the mesh resolution with $\Delta l = 0.025 d_b$ presents little deviation from the finer resolution. Therefore, the simulations were performed with $\Delta l = 0.025 d_b$.

3.3 Comparison with the literature

From the spherical and almost spherical (for high Re values the morphology slightly deviates from a sphere) cases presented ($Eo = 1.0$), the numerical results presented here were compared with correlations found in literature (Ranz and Marshall, 1952; Lochiel and Calderbank, 1964; LeClair and Hamielec, 1971; Oellrich *et al.*, 1973; Takemura and Yabe, 1998). This comparison is shown in Fig. 5 for $Pr = 10.0$ through the Nusselt number Nu_{global} plotted against the obtained Re and Pe ($Pe = RePr$) numbers.

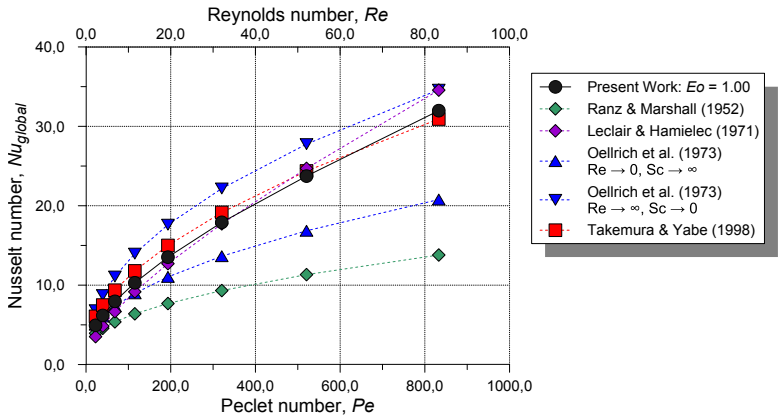

Figure 5. Nusselt Nu_{global} values against Reynolds Re and Pe numbers obtained in the present work from correlations found in literature for $Pr = 10.0$.

From Fig. 5 it is possible to observe the behavior of the proposed equations found in literature and the values obtained in this work for $Pr = 10.0$ and how they deviate from one to another. It also shows that an increase in the Reynolds Re number provokes an increase in the Nusselt Nu_{global} number and $Nu_{global} \to 2.0$ for $Re \to 0$, the value for pure diffusive heat transfer.

The (Ranz and Marshall, 1952) correlation present a large deviation from the results of this work, the explanation lies in the fact that the correlation was proposed for drops and not for bubbles. However, it is show here due to its simple form, composed by two additive terms, one for diffusion and other for the forced convection heat or mass transfer. The correlation proposed by (Lochiel and Calderbank, 1964) shows certain agreement when Pe is large, since the equation apply only for high Pe and Pr (Sc). On the contrary, the equation given by (Oellrich *et al.*, 1973) agrees well in the low Pe and low Re region, since the correlation is suitable for this range of Re values (Clift *et al.*, 1978). The values presented here show a good agreement with the correlations of LeClair and Hamielec (1971) due to the its applicability until $Re < 100$. For the Nu_{global} values calculated from Takemura and Yabe (1998), the results presents very good agreement in the range where the use of the correlation is presented, $Re < 100$ and $Pe > 1$.

The results presented in section 3.2 and here, specially the agreement of the results with Takemura and Yabe (1998), endorses the fact that the methodology utilized in the present work captures well the interfacial and can be used for more sophisticated studies.

3.4 Local Heat Transfer

The local analysis is made with results of the red points of Fig. 3, which obtained similar Re number, for different Eo numbers, in order to see the effect of distortion and the fluid thermal properties (Pr) in the interfacial heat transfer around the fluid particle. Therefore, Fig. 7 shows the fluid particle shape, temperature and the external flow streamlines, after reaching the steady-state regime, for four different configurations and three Prandtl Pr numbers ($Pr = 0.25$, $Pr = 1.0$, $Pr = 10.0$). The morphologies can be classified as the following: i) spherical shape ($Eo = 1.0, \log(Mo) = -5.29$); ii) ellipsoidal shape ($Eo = 5.0, \log(Mo) = -3.86$ and $Eo = 10.0, \log(Mo) = -3.21$); and iii) ellipsoidal-cap shape ($Eo = 40.0, \log(Mo) = -1.5$).

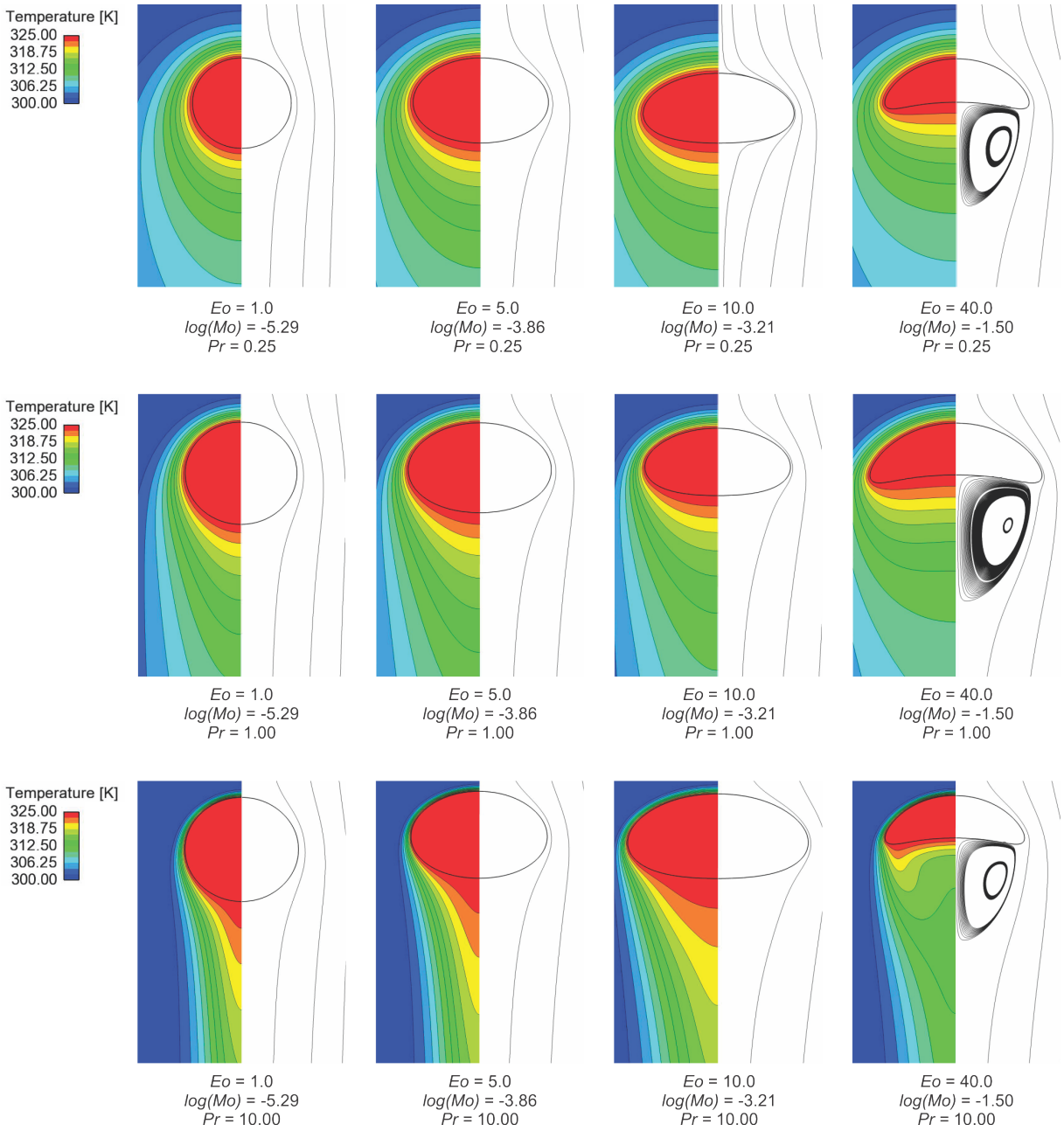

Figure 6. Fluid particle shapes, temperature contours and the streamlines around it, after reaching the steady-state regime three Prandtl Pr numbers ($Pr = 0.25$, $Pr = 1.0$, $Pr = 10.0$). The images are not in scale.

Figure 6 gives a visual insight of how the deformation (deviation from the spherical shape) affects the temperature field and flow around the fluid particle. As the deformation increases (higher Eo) a recirculation zone starts to appear in the rear.

The effect of the Pr number on the temperature around the bubble can be noticed by the thinning of the temperature distribution as the Pr increases, since it gives a relation between the momentum and thermal boundary layer thickness.

On the rear, for the situations where the fluid particle is spherical and elliptical, the temperature distribution thins in the radial direction and enlarges in the axial direction, as seen by the contour lines. However, for $Eo = 40.0$, the contour lines present a different behavior, a temperature peak begins to appear near the point where the curvature changes due to the recirculation zone.

The changes on the temperature field can be easily understand by seeing the situation by the means of the Pe number, the ratio of convective and diffusive transport. Since the dimensionless number is given by the product of Re and Pr, as Pr increases, the Pe also increases. Then, the convective heat transport starts to be dominant, meaning that the energy transport becomes to more dependent of the velocity field around the fluid particle, explaining the changes on the temperature distribution. This effect is more evident for the situation with $Eo = 40.0$ and $Pr = 10.0$, where the temperature distribution on the rear is highly affected by the recirculation zone when comparing to the other cases.

In order to show how the deviation from a spherical shape and the velocity field near the interface affects the heat transfer, Fig. 7 gives the normalized Nusselt number Nu^* and normalized tangential interface velocity ${u_t}^*$ around the bubble with the aid of the dimensionless distance s^*, these denoted by:

$$s^* = \frac{s}{s_{\max}}; \tag{13}$$

$$Nu^* = \frac{Nu_{\text{local}} - Nu_{\min}}{Nu_{\max} - Nu_{\min}}; \tag{14}$$

$${u_t}^* = \frac{|u_{t\text{local}}|}{u_{t\max}}; \tag{15}$$

where $\vec{t}$ is the tangential interface vector of bubble interface and the subscripts loc, min and max refers respectively to the local, minimum and maximum local values.

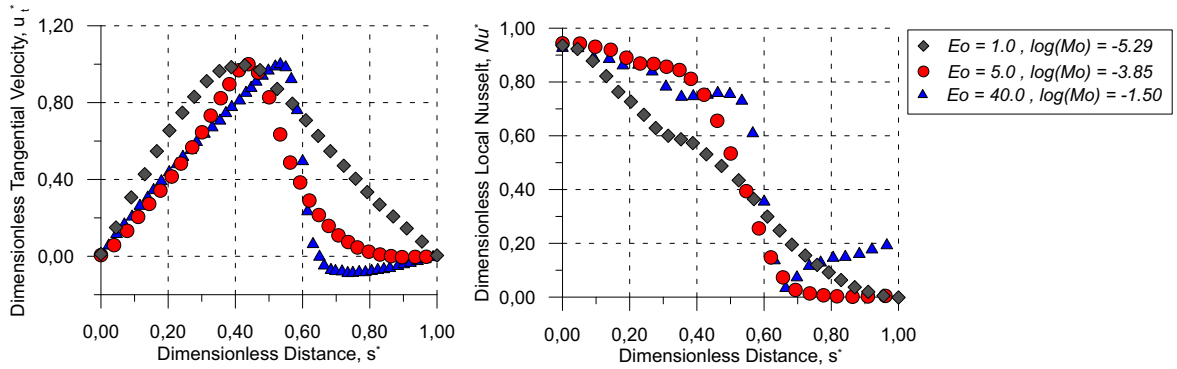

Figure 7. Normalized tangential interface velocity ${u_t}^*$ and Nusselt number Nu^* around the bubble. These profiles were extracted for the situations given in Fig. 6 with $Pr = 10.0$.

From Fig. 7, it is clearly visible changes in the s^* *vs.* ${u_t}^*$ and Nu^* *vs.* ${u_t}^*$ plots as the fluid particle is distorted from spherical ($Eo = 1.0$) to ellipsoidal ($Eo = 5.0$) and ellipsoidal-cap ($Eo = 40.0$). The s^* *vs.* ${u_t}^*$ plot, shows two distinct regions in all situations, separated by a point where ${u_t}^*$ is maximum. As Eo increases, this peak start to moves down to the rear portion of the fluid particle and ${u_t}^*$ profiles of this portion tends to show lower values. For $Eo = 40.0$, the ${u_t}^*$ profile in the rear portion gives negative values, due to an recirculation region.

The changes in the s^* *vs.* ${u_t}^*$ are reflected in the s^* *vs.* Nu^* curves. For $Eo = 1.0$, where the fluid particle is spherical, the local interfacial heat transfer decays smoothly from a maximum value in the bubble front ($s^* = 0.00$) to a minimum in the rear end ($s^* = 1.00$) and there is no large contrast dividing the front and rear portion as the ${u_t}^*$ profile. Increasing the Eo, $Eo = 5.0$, the Nu^* profile changes, showing now a transition region from $s^* \approx 0.40$ to $s^* \approx 0.70$, where the interfacial heat transfer is increased in the front region and decreased in the rear part, as expect from the ${u_t}^*$ curve. In the last situation, $Eo = 40.0$, again there is a transition in the Nu^* profile from $s^* \approx 0.50$ to $s^* \approx 0.70$, yet now in the rear part, the fluid recirculation makes the interafacial heat transfer achieve a minimum value near $s^* \approx 0.70$ to then increase.

3.5 Total Heat Transfer

The results from the sections 3.2 and 3.3 brings reliability on the model hereby implemented. Thus, it can be used to study the situation of deformed fluid particles. Fig. 8 shows the effect of the Eötvös Eo number in the Nu *vs.* Re curve for different Pr numbers.

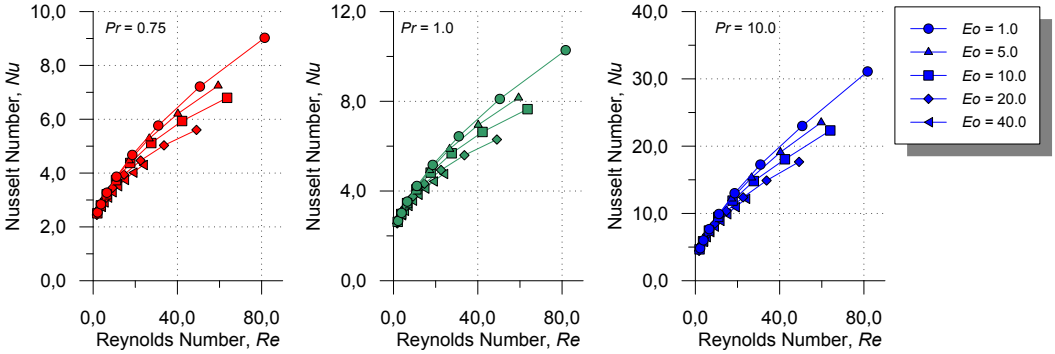

Figure 8. Effect of the Eötvös Eo number in the Re *vs.* Nu curve for different Pr numbers.

As expected, the increase in the Reynolds Re number provokes an increase in the Nusselt Nu number and $Nu \to 2.0$ for $Re \to 0$, the value for pure diffusive heat transfer. The effect of the Pr in the Fig. 8 creates an augmentation of the interfacial heat transfer, once this dimensionless parameter gives the relation beetween the thermal and momemntum boundary layer as commented in section 3.2 . Besides the increase in the interfacial heat transfer, Fig. 8 also shows that the increase of the Pr number reduces the impact of the deformation, here seen by the Eo lines. As Pr increases, these lines begin to become nearer, demonstrating that the effect of Pr number is not linear for some fluid particle morphologies.

In order to see this effect, the results were compared through another curve, Nu *vs.* Pe, given by Fig. 9.

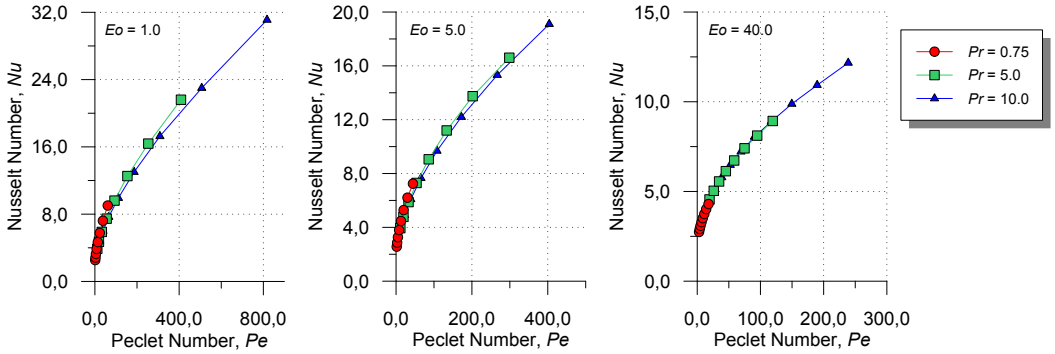

Figure 9. Effect of the Prandtl Pr number in the Pe *vs.* Nu curve for different Eo numbers.

Figure 9 shows that the Pe *vs.* Nu lines begin to coincide as the Eo number increases, i.e., the fluid particle deformation, from spherical to spherical-cap. This same behavior is encountered the work of Oellrich *et al.* (1973), where for spherical bubbles the Sc *vs.* Pe values do not coincide for different Sc numbers, giving an upper ($Sc \to \infty$) and a lower ($Sc \to 0$) limit. From the results showed in section 3.4 , this effect is explained by boundary layer separation location and the formation of the recirculation zone behind the particle, all due to the interfacial changes.

To quantify the fluid particle deformation, the surface ratio S_{ratio} (Eq. (16)) is employed,

$$S_{ratio} = \frac{S}{S_{sphere}}, \tag{16}$$

which is the relation of the obtained surface area S with an iso-surface of $\alpha_b = 0.1$ (see Fig. 1) in the steady state with the surface area of a sphere ($S_{sphere} = \pi {d_b}^2$). In this manner, Figure 10 illustrates how the balance of the inertial, viscous, and superficial forces affects the interfacial surface, i.e., the contact area between the fluid phases.

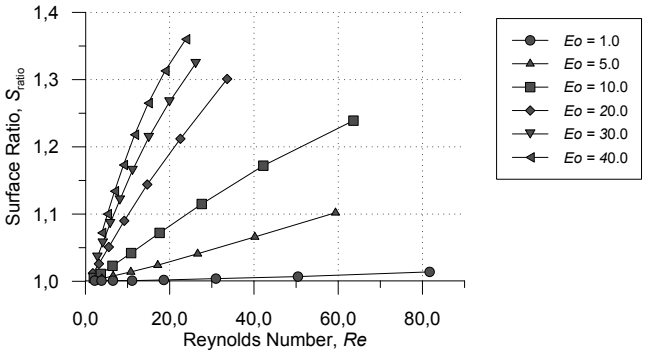

Figure 10. S_{ratio} *vs.* Re values for different Eo numbers.

The illustration above indicates that increase of the interfacial surface is higher when the superficial forces are not and c dominant (higher Eo) cannot be neglected in the heat or mass transfer, since there is a considerable variation in the values. This effect needs to be introduced in classical the Two-Fluid Model, since it is usual to express the interfacial heat transfer q_i'' as,

$$q_i'' = h a_i''' \Delta T, \tag{17}$$

where a_i''' is the interfacial area density. The interfacial area density a_i''' is the variable that gives the information about the fluid particle interface. This value is usually given assuming that the dispersed phase is spherical shaped, specially when modeling bubbly flows, so for a spherical fluid particle,

$$a_i''' = \alpha_b \frac{S_b}{V_b} = \alpha_b \frac{\pi d_b^2}{\pi d_b^3/6} = \frac{6\alpha_b}{d_b}. \tag{18}$$

However, the fluid particle may not be spherically shaped in several real applications. To introduce this factor in Eq. (18), the following correction factor $f_\chi(Re, Eo)$ is introduced,

$$a_i''' = \alpha_b \frac{S}{V_b} = \alpha_b \frac{S}{V_b}\frac{S_b}{S_b} = \alpha_b \frac{S_b}{V_b}\frac{S}{S_b} = \alpha_b \frac{S_b}{V_b} S_{ratio} = \frac{6\alpha_b}{d_b} S_{ratio} = \frac{6\alpha_b}{d_b} f_\chi(Re, Eo). \tag{19}$$

where, $f_\chi(Re, Eo) = S_{ratio}$.

For this reason, rewriting Eq. (17) and taking the convective heat transfer coefficient as $h = Nu(Re, Eo, Pr)\, k_c/d_b$, the interfacial heat tranfer q_i'' can be expressed as,

$$q_i'' = Nu(Re, Eo, Pr)\frac{k_c}{d_b}\frac{6\alpha_b}{d_b} f_\chi(Re, Eo)\Delta T, \tag{20}$$

which computes the effects presented in Figs. 8 and 10.

In the interest investigate these two effects, Fig. 11 gives the value of $q_i''/\Delta T$, taking the product $\dfrac{k_c}{d_b}\dfrac{6\alpha_b}{d_b}$ as unity, for different Eo and Pr numbers.

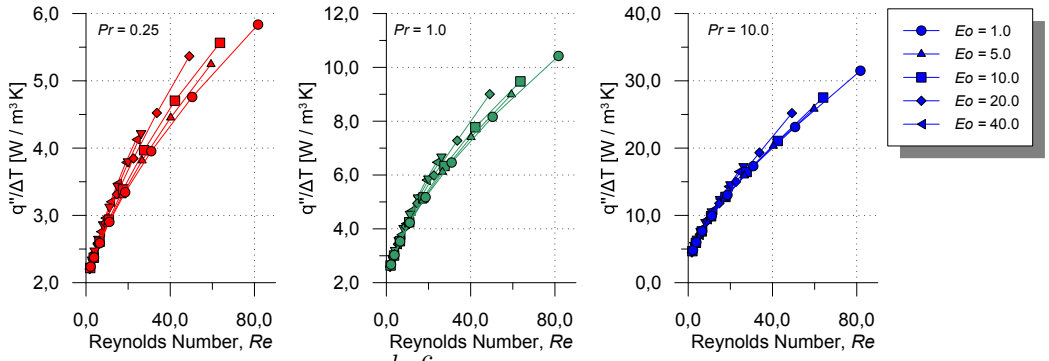

Figure 11. value of $q_i''\Delta T$, with $\dfrac{k_c}{d_b}\dfrac{6\alpha_b}{d_b} = 1.0\, W/m^3K$, for different Eo and Pr numbers.

As it can be seen, when accounting the changes in the interfacial surface, the fluid particle deformation increases the heat transfer. However, this effect of the deformation tends to decrease as Pr increases. The reason for that particular behavior is explained by the analysis presented in Fig. 8 and 9, where for low Eo, the Pr varies in a non-linear fashion, then making the lower Eo curves to gather into a single curve.

4. CONCLUSIONS

In this work the interfacial heat transfer of spherical and distorted fluid particles was studied with the Volume-Of-Fluid (VOF) model available in ANSYS CFD FLUENT 15.0. The governing equations were solved for a moving reference frame, including the effect of the bubble acceleration trough a source term in the momentum conservation equation, implemented via FLUENTs User Define Functions (UDF).

It is shown that is difficult to evaluate temperatures and fluxes in the interface, due to shortcoming of the interface tracking through implicit methods, although the values obtained in this fashion present qualitative results. In order to compensate for this fact, the temperature in the dispersed phase (fluid particle) is maintained constant through an energy source term added via FLUENTs User Define Functions (UDF). With the aid this source term is possible to calculate the interfacial heat transfer and to develop studies from different bubble regimes.

The methodology utilized in the present work capture well the interfacial transfer, once the mesh refinement study shows that the boundary and momentum boundary layer are captured and the dimensionless values obtained (Nu and Re) agree well with correlations encountered in the literature(Ranz and Marshall, 1952; Lochiel and Calderbank, 1964; LeClair and Hamielec, 1971; Oellrich *et al.*, 1973; Takemura and Yabe, 1998) for spherical fluid particles.

Through a detailed modeling and analysis of the flow around fluid particles with different shapes it was possible to possible to perceive changes in the thermal and flow behavior as the deviation from a spherical shape increases.

The results show that the deformation, not accounting the changes in interfacial contact area, decreases the total interfacial heat transfer and the Nu or Sh values are independent of Pr or Sc values when the fluid particle is distorted.

In order to investigate the effects of the changes in the interfacial contact area due the distortion in the heat transfer, the results are presented in the Two-Fluid Model (TFM) perspective. In this point of view, the fluid particle deformation increases the interfacial heat transfer with this effect decreasing as Pr increases.

5. ACKNOWLEDGEMENTS

This work was realized with the financial support of the Brazilian National Petroleum Agency - ANP , through Human Resources Program of ANP for Petroleum and Natural Gas.

6. REFERENCES

Aboulhasanzadeh, B., Hosoda, S., Tomiyama, A. and Tryggvason, G., 2013. "A validation of an embedded analytical description approach for the computations of high schmidt number mass transfer from bubbles in liquids". *Chemical Engineering Science*, Vol. 101, pp. 165–174.

Aboulhasanzadeh, B., Thomas, S., Taeibi-Rahni, M. and Tryggvason, G., 2012. "Multiscale computations of mass transfer from buoyant bubbles". *Chemical Engineering Science*, Vol. 75, pp. 456–467.

Bothe, D. and Fleckenstein, S., 2013. "A volume-of-fluid-based method for mass transfer processes at fluid particles". *Chemical Engineering Science*, Vol. 101, No. 0, pp. 283 – 302.

Brackbill, J., Kothe, D.B. and Zemach, C., 1992. "A continuum method for modeling surface tension". *Journal of computational physics*, Vol. 100, No. 2, pp. 335–354.

Clift, R., Grace, J. and Weber, M., 1978. "Bubbles". *Drops and Particles (Academic, New York, 1978)*, p. 1870.

Figueroa-Espinoza, B. and Legendre, D., 2010. "Mass or heat transfer from spheroidal gas bubbles rising through a stationary liquid". *Chemical Engineering Science*, Vol. 65, No. 23, pp. 6296–6309.

Hase, M. and Weigand, B., 2004. "Transient heat transfer of deforming droplets at high reynolds numbers". *International Journal of Numerical Methods for Heat & Fluid Flow*, Vol. 14, No. 1, pp. 85–97.

Hayashi, K., Hosoda, S., Tryggvason, G. and Tomiyama, A., 2014. "Effects of shape oscillation on mass transfer from a taylor bubble". *International Journal of Multiphase Flow*, Vol. 58, pp. 236–245.

Hirt, C.W. and Nichols, B.D., 1981. "Volume of fluid (vof) method for the dynamics of free boundaries". *Journal of computational physics*, Vol. 39, No. 1, pp. 201–225.

Ishii, M. and Hibiki, T., 2011. *Thermo-fluid dynamics of two-phase flow*. Springer.

Kantarci, N., Borak, F. and Ulgen, K.O., 2005. "Bubble column reactors". *Process Biochemistry*, Vol. 40, No. 7, pp. 2263–2283.

Lafaurie, B., Nardone, C., Scardovelli, R., Zaleski, S. and Zanetti, G., 1994. "Modelling merging and fragmentation in multiphase flows with {SURFER}". *Journal of Computational Physics*, Vol. 113, No. 1, pp. 134 – 147.

LeClair, B. and Hamielec, A., 1971. "Viscous flow through particle assemblages at intermediate reynolds numbers – a cell model for transport in bubble swarms". *The Canadian Journal of Chemical Engineering*, Vol. 49, No. 6, pp. 713–720.

Lochiel, A. and Calderbank, P., 1964. "Mass transfer in the continuous phase around axisymmetric bodies of revolution". *Chemical Engineering Science*, Vol. 19, No. 7, pp. 471–484.

Marschall, H., Hinterberger, K., Schueler, C., Habla, F. and Hinrichsen, O., 2012. "Numerical simulation of species transfer across fluid interfaces in free-surface flows using openfoam". *Chemical Engineering Science*, Vol. 78, pp.

111–127.

Oellrich, L., Schmidt-Traub, H. and Brauer, H., 1973. "Theoretische berechnung des stofftransports in der umgebung einer einzelblase". *Chemical Engineering Science*, Vol. 28, No. 3, pp. 711–721.

Ranz, W. and Marshall, W., 1952. "Evaporation from drops". *Chem. Eng. Prog*, Vol. 48, No. 3, pp. 141–146.

Takemura, F. and Yabe, A., 1998. "Gas dissolution process of spherical rising gas bubbles". *Chemical engineering science*, Vol. 53, No. 15, pp. 2691–2699.

Wang, J., Lu, P., Wang, Z., Yang, C. and Mao, Z.S., 2008. "Numerical simulation of unsteady mass transfer by the level set method". *Chemical Engineering Science*, Vol. 63, No. 12, pp. 3141–3151.

Youngs, D.L., 1982. "Time-dependent multi-material flow with large fluid distortion". *Numerical methods for fluid dynamics*, Vol. 24, pp. 273–285.

7. RESPONSIBILITY NOTICE

The authors are the only responsible for the printed material included in this paper.